Gains and Limits of MIMO Technology for Safety-Critical PLC Applications

Leyna Sadamori*, Thomas Hunziker† and Stephen Dominiak†
*ETH Zurich, Department of Computer Science
Universitätstr. 6, 8092 Zürich, Switzerland
†Lucerne University of Applied Sciences and Arts
Technikumstr. 21, 6048 Horw, Switzerland
Email: leyna.sadamori@inf.ethz.ch, {thomas.hunziker, stephen.dominiak}@hslu.ch

***Abstract*—Many Power Line Communication (PLC) systems operate on top of multi-conductor infrastructures, which allows for the adoption of Multiple Input Multiple Output (MIMO) techniques. Current channel models for MIMO PLC do not consider terminal conditions and are focused on optimizing the average case. For safety-critical applications, however, the line terminations are important, as system performance has to be guaranteed for any conditions—including the worst case.**

In this paper, we present an analytical and a SPICE[1]-simulated channel model based on transmission line theory that is capable of incorporating terminal networks. Further, we evaluate the channel capacity and compare three different systems that could be deployed in a multi-conductor environment: A Single Input Single Output (SISO) system, multiple parallel SISO systems and a MIMO system. With our channel model we show that the terminal conditions have an impact on the overall signal attenuation, but also that they affect the relative cross-talk level compared to direct channels. Although we can confirm existing findings that MIMO techniques do provide performance gains, our results show that this is only true above a certain signal-to-noise ratio (SNR). For low SNRs, these gains decrease and in worst case, the gains over a SISO system are lost. Also, parallel SISO systems do not offer robust performance gains over single SISO systems, which discourages their use for safety-critical applications.

I. Introduction

The adoption of Multiple Input Multiple Output (MIMO) techniques to Power Line Communication (PLC) systems has recently gained momentum, mainly for two reasons: Most PLC systems run on top of a multi-conductor infrastructure, which is the physical basis for the adoption of MIMO techniques. Second, MIMO techniques have already proven their benefits in widely used wireless technologies such as IEEE 802.11n or LTE. The application of MIMO in the PLC domain has already been investigated, however, mainly for in-home scenarios [1]–[3]. Even though MIMO is successfully deployed in wireless technologies, its adoption to the PLC domain is currently limited to non-safety-critical environments such as in-home applications. Safety-critical PLC applications, e.g., the medium-voltage power grid [4] or avionics systems [5], have stricter performance requirements, as system performance has to be guaranteed for any conditions—including the worst case.

[1]Simulation Program with Integrated Circuit Emphasis

A fundamental part in understanding the gains and limits of MIMO for safety-critical PLC applications is a proper channel model. A common way to classify (Single Input Single Output (SISO)) channel models is to distinguish between empirical (or phenomenological) and deterministic models [6], [7]. Empirical models consider the channel as a black box with the same input/output behavior as the real channel, whereas deterministic models make use of well-known physical models for electro-magnetic (EM) wave propagation. The difference of the two approaches lies in the two competing aspects *generality* versus *specificity*, and *complexity* versus *simplicity*. Empirical models can be applied to arbitrarily complex network topologies (simplicity), but they are specific to it (specificity). Deterministic models can be built for any network topologies (generality), if all the physical properties are known (complexity). The underlying theory for deterministic channel models is transmission line theory, multi-conductor transmission line (MTL) theory in case of MIMO channels.

In this paper, we present an extension to existing MTL-based channel models [8], [9] by incorporating terminal networks. A PLC system under operating conditions will face terminal mismatches due to dynamically changing loads. By incorporating the terminal networks into our channel model, we obtain better insights into the impact of these mismatches, which is necessary for worst-case considerations in safety-critical applications. We present an analytical and a SPICE-simulated approach, where the latter provides the possibility to also model effects of devices such as signal couplers or impedance transformers. Finally, we address the question whether MIMO techniques do provide gains in safety-critical PLC applications. To do so, we compare the performance of a MIMO system against multiple parallel SISO systems, and a single SISO system, which are all systems that could potentially be deployed on a multi-conductor PLC infrastructure.

II. From MTL Theory to the Channel Model

The basis of our deterministic channel model is MTL theory, a well-known simplification of the Maxwell equations for EM waves that are guided by conducting material [10]. Assuming a wire with $n+1$ conductors, we can define n independent voltages and currents $\hat{V}_i(z)$ and $\hat{I}_i(z), i \in \{1,\dots,n\}$ in the frequency domain (indicated by phasor notation $\hat{\{\cdot\}}$), where

z denotes the coordinate along the transmission line. The telegrapher's equations in the frequency-domain are given as

$$\frac{d}{dz}\hat{\boldsymbol{V}}(z) = -\hat{\boldsymbol{Z}}\hat{\boldsymbol{I}}(z) \tag{1a}$$

$$\frac{d}{dz}\hat{\boldsymbol{I}}(z) = -\hat{\boldsymbol{Y}}\hat{\boldsymbol{V}}(z), \tag{1b}$$

with

$$\hat{\boldsymbol{Z}} = \boldsymbol{R} + j\omega\boldsymbol{L} \tag{2a}$$

$$\hat{\boldsymbol{Y}} = \boldsymbol{G} + j\omega\boldsymbol{C}, \tag{2b}$$

where $\hat{\boldsymbol{V}}(z)$ and $\hat{\boldsymbol{I}}(z)$ denote the $n \times 1$ vectors holding the n voltages and currents, and $\boldsymbol{R}, \boldsymbol{L}, \boldsymbol{G}$ and $\boldsymbol{C}$ denote the per-unit-length (p.u.l.) parameter matrices of the line. In order to decouple the first-order differential equations in (1), we take the derivative and substitute them by the other, which yields

$$\frac{d^2}{dz^2}\hat{\boldsymbol{V}}(z) = \hat{\boldsymbol{Z}}\hat{\boldsymbol{Y}}\hat{\boldsymbol{V}}(z) \tag{3a}$$

$$\frac{d^2}{dz^2}\hat{\boldsymbol{I}}(z) = \hat{\boldsymbol{Y}}\hat{\boldsymbol{Z}}\hat{\boldsymbol{I}}(z). \tag{3b}$$

We can now introduce a change of variables

$$\hat{\boldsymbol{V}}(z) = \hat{\boldsymbol{T}}_V\hat{\boldsymbol{V}}_m(z) \tag{4a}$$

$$\hat{\boldsymbol{I}}(z) = \hat{\boldsymbol{T}}_I\hat{\boldsymbol{I}}_m(z) \tag{4b}$$

and insert them into (3), which yields

$$\frac{d^2}{dz^2}\hat{\boldsymbol{V}}_m(z) = \hat{\boldsymbol{T}}_V^{-1}\hat{\boldsymbol{Z}}\hat{\boldsymbol{Y}}\hat{\boldsymbol{T}}_V\hat{\boldsymbol{V}}_m(z) \tag{5a}$$

$$\frac{d^2}{dz^2}\hat{\boldsymbol{I}}_m(z) = \hat{\boldsymbol{T}}_I^{-1}\hat{\boldsymbol{Y}}\hat{\boldsymbol{Z}}\hat{\boldsymbol{T}}_I\hat{\boldsymbol{I}}_m(z). \tag{5b}$$

We may write $\hat{\boldsymbol{T}}_V^{-1}\hat{\boldsymbol{Z}}\hat{\boldsymbol{Y}}\hat{\boldsymbol{T}}_V = \hat{\boldsymbol{T}}_I^{-1}\hat{\boldsymbol{Y}}\hat{\boldsymbol{Z}}\hat{\boldsymbol{T}}_I = \hat{\gamma}^2$, which is of the form $\boldsymbol{T}^{-1}\boldsymbol{M}\boldsymbol{T} = \boldsymbol{\Lambda}$, also known as the eigenvalue problem. We obtain $\hat{\boldsymbol{T}}_V$, $\hat{\boldsymbol{T}}_I$ and $\hat{\gamma}^2$ through eigenvalue decomposition, and obtain decoupled mode quantities $\hat{\boldsymbol{V}}_m(z), \hat{\boldsymbol{I}}_m(z)$, since $\hat{\gamma}^2$ is a diagonal matrix. The equations for the decoupled mode quantities have the simple solution [10]

$$\hat{\boldsymbol{V}}_m(z) = \boldsymbol{e}^{-\hat{\gamma}z}\hat{\boldsymbol{V}}_m^{+} + \boldsymbol{e}^{\hat{\gamma}z}\hat{\boldsymbol{V}}_m^{-} \tag{6a}$$

$$\hat{\boldsymbol{I}}_m(z) = \boldsymbol{e}^{-\hat{\gamma}z}\hat{\boldsymbol{I}}_m^{+} - \boldsymbol{e}^{\hat{\gamma}z}\hat{\boldsymbol{I}}_m^{-}, \tag{6b}$$

with

$$\boldsymbol{e}^{\pm\hat{\gamma}z} = \begin{bmatrix} e^{\pm\hat{\gamma}_1 z} & \dots & 0 \\ \vdots & \ddots & \vdots \\ 0 & \dots & e^{\pm\hat{\gamma}_n z} \end{bmatrix}. \tag{7}$$

The unknown coefficients in $\hat{\boldsymbol{V}}_m^{\pm}$ and $\hat{\boldsymbol{I}}_m^{\pm}$ in (6) add up to $4n$ unknowns.

We can reduce the number of unknowns down to $2n$ by substituting (6b) into (4b), and using the relations from (1b):

$$\begin{aligned}\hat{\boldsymbol{V}}(z) &= \hat{\boldsymbol{Y}}^{-1}\hat{\boldsymbol{T}}_I\hat{\gamma}\left(\boldsymbol{e}^{-\hat{\gamma}z}\hat{\boldsymbol{I}}_m^{+} + \boldsymbol{e}^{\hat{\gamma}z}\hat{\boldsymbol{I}}_m^{-}\right) \\ &= \underbrace{\hat{\boldsymbol{Y}}^{-1}\hat{\boldsymbol{T}}_I\hat{\gamma}\hat{\boldsymbol{T}}_I^{-1}}_{\hat{\boldsymbol{Z}}_C}\hat{\boldsymbol{T}}_I\left(\boldsymbol{e}^{-\hat{\gamma}z}\hat{\boldsymbol{I}}_m^{+} + \boldsymbol{e}^{\hat{\gamma}z}\hat{\boldsymbol{I}}_m^{-}\right)\end{aligned} \tag{8a}$$

$$\hat{\boldsymbol{I}}(z) = \hat{\boldsymbol{T}}_I\left(\boldsymbol{e}^{-\hat{\gamma}z}\hat{\boldsymbol{I}}_m^{+} - \boldsymbol{e}^{\hat{\gamma}z}\hat{\boldsymbol{I}}_m^{-}\right), \tag{8b}$$

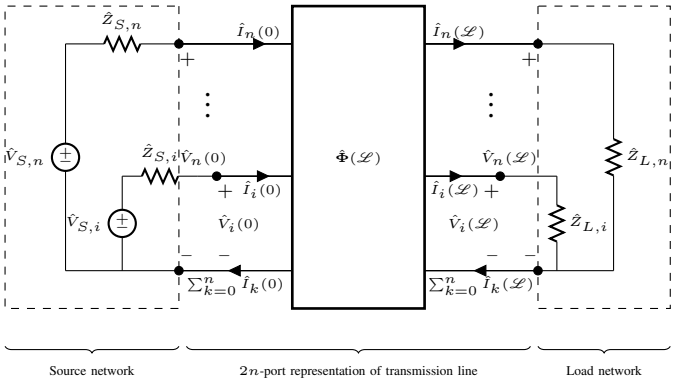

Fig. 1: Channel model for a MIMO PLC channel with $n+1$ conductors. The channel is modeled by a $2n$-port representation of the transmission line. Transmitter and receiver are modeled by source and load networks.

where we introduce $\hat{\boldsymbol{Z}}_C$ as the characteristic impedance matrix of the line.

A. $2n$-Port Representation

The $2n$-port representation of a transmission line gives a simple matrix notation that relates the voltages and currents at the output to the input of the network. We choose the chain-parameter representation for our channel model, for which the following relationship holds:

$$\begin{bmatrix}\hat{\boldsymbol{V}}(0) \\ \hat{\boldsymbol{I}}(0)\end{bmatrix} = \underbrace{\begin{bmatrix}\hat{\boldsymbol{\Phi}}_{11} & \hat{\boldsymbol{\Phi}}_{12} \\ \hat{\boldsymbol{\Phi}}_{21} & \hat{\boldsymbol{\Phi}}_{22}\end{bmatrix}}_{\hat{\boldsymbol{\Phi}}(\mathscr{L})}\begin{bmatrix}\hat{\boldsymbol{V}}(\mathscr{L}) \\ \hat{\boldsymbol{I}}(\mathscr{L})\end{bmatrix}, \tag{9}$$

where $\hat{\boldsymbol{\Phi}}(\mathscr{L})$ denotes the chain-parameter matrix for a line segment of length $\mathscr{L}$. Using the solutions for the line voltages and currents in (8) and inserting them in (9), we obtain

$$\hat{\boldsymbol{\Phi}}_{11} = \frac{1}{2}\hat{\boldsymbol{Z}}_C\hat{\boldsymbol{T}}_I\left(\boldsymbol{e}^{\hat{\gamma}\mathscr{L}} + \boldsymbol{e}^{-\hat{\gamma}\mathscr{L}}\right)\hat{\boldsymbol{T}}_I^{-1}\hat{\boldsymbol{Z}}_C^{-1} \tag{10a}$$

$$\hat{\boldsymbol{\Phi}}_{12} = \frac{1}{2}\hat{\boldsymbol{Z}}_C\left[\hat{\boldsymbol{T}}_I\left(\boldsymbol{e}^{\hat{\gamma}\mathscr{L}} - \boldsymbol{e}^{-\hat{\gamma}\mathscr{L}}\right)\hat{\boldsymbol{T}}_I^{-1}\right] \tag{10b}$$

$$\hat{\boldsymbol{\Phi}}_{21} = \frac{1}{2}\left[\hat{\boldsymbol{T}}_I\left(\boldsymbol{e}^{\hat{\gamma}\mathscr{L}} - \boldsymbol{e}^{-\hat{\gamma}\mathscr{L}}\right)\hat{\boldsymbol{T}}_I^{-1}\right]\hat{\boldsymbol{Z}}_C^{-1} \tag{10c}$$

$$\hat{\boldsymbol{\Phi}}_{22} = \frac{1}{2}\hat{\boldsymbol{T}}_I\left(\boldsymbol{e}^{\hat{\gamma}\mathscr{L}} + \boldsymbol{e}^{-\hat{\gamma}\mathscr{L}}\right)\hat{\boldsymbol{T}}_I^{-1}. \tag{10d}$$

B. Channel Transfer Function

The channel transfer function (CTF) of a $N_r \times N_t$ MIMO channel can be written as a $N_r \times N_t$ channel matrix $\boldsymbol{H}$, whose entries $h_{ij}, i \in \{1, \dots, N_r\}, j \in \{1, \dots, N_t\}$ correspond to the complex-valued, frequency-dependent channel gains[2] between the j-th transmitter and i-th receiver. For a multi-conductor infrastructure with $n+1$ conductors, we have $N_r = N_t = n$.

[2]Note that the CTF is generally complex-valued and frequency-dependent. For simplicity, we omit both the phasor notation and frequency dependency in the communications domain.

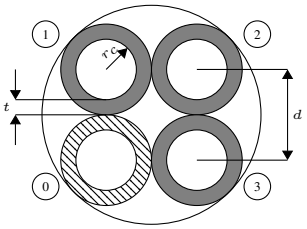

Fig. 2: Cross-sectional dimensions of cable bundle with 3 phases (grey insulation, $i \in \{1, 2, 3\}$) and common return (striped insulation, $i = 0$), conductor radius r_c, insulation thickness t and conductor distance $d = 2(r_c + t)$.

We model the MIMO PLC channel as a sequence of transmitter, transmission line, and receiver, as depicted in Fig. 1. The transmitters are modeled as voltage sources $\hat{\boldsymbol{V}}_S$ with source impedances $\hat{\boldsymbol{Z}}_S$, the receivers as load networks $\hat{\boldsymbol{Z}}_L$ and the transmission lines by their $2n$-port representation. We define our CTF as the ratio of the voltages at the load to the source voltages, also known as insertion loss, which can be written as

$$\hat{\boldsymbol{V}}(\mathscr{L}) = \boldsymbol{H} \cdot \hat{\boldsymbol{V}}_S. \tag{11}$$

Using the $2n$-port relations from (9), we can first substitue the terminal conditions $\hat{\boldsymbol{V}}(0) = \hat{\boldsymbol{V}}_S - \hat{\boldsymbol{Z}}_S \hat{\boldsymbol{I}}(0)$ at the transmitter, which yields

$$\hat{\boldsymbol{\Phi}}_{11}\hat{\boldsymbol{V}}(\mathscr{L}) + \hat{\boldsymbol{\Phi}}_{12}\hat{\boldsymbol{I}}(\mathscr{L}) = \hat{\boldsymbol{V}}_S - \hat{\boldsymbol{Z}}_S \left[\hat{\boldsymbol{\Phi}}_{21}\hat{\boldsymbol{V}}(\mathscr{L}) + \hat{\boldsymbol{\Phi}}_{22}\hat{\boldsymbol{I}}(\mathscr{L})\right], \tag{12}$$

and then substitute the terminal conditions $\hat{\boldsymbol{V}}(\mathscr{L}) = \hat{\boldsymbol{Z}}_L \hat{\boldsymbol{I}}(\mathscr{L})$ at the receiver and obtain

$$\left[\hat{\boldsymbol{\Phi}}_{11} + \hat{\boldsymbol{\Phi}}_{12}\hat{\boldsymbol{Z}}_L^{-1}\right] \hat{\boldsymbol{V}}(\mathscr{L}) = \hat{\boldsymbol{V}}_S - \hat{\boldsymbol{Z}}_S \left[\hat{\boldsymbol{\Phi}}_{21} + \hat{\boldsymbol{\Phi}}_{22}\hat{\boldsymbol{Z}}_L^{-1}\right] \hat{\boldsymbol{V}}(\mathscr{L}). \tag{13}$$

With the definition from (11), we can now write the CTF as

$$\boldsymbol{H} = \left(\hat{\boldsymbol{\Phi}}_{11} + \hat{\boldsymbol{\Phi}}_{12}\hat{\boldsymbol{Z}}_L^{-1} + \hat{\boldsymbol{Z}}_S\hat{\boldsymbol{\Phi}}_{21} + \hat{\boldsymbol{Z}}_S\hat{\boldsymbol{\Phi}}_{22}\hat{\boldsymbol{Z}}_L^{-1}\right)^{-1}. \tag{14}$$

C. Computation of the Per-Unit-Length Parameters

In order to compute the CTF as described above, we need to determine the p.u.l. parameters of the transmission line. We use closed-form solutions and therefore assume a homogenous dielectric surrounding of the conductors (enclosed air and outer sheath are neglected). Furthermore, we neglect internal inductances and polarization losses. Gruber and Lampe present a study on the impact of these simplifications [9].

As an exemplary safety-critical scenario, we choose an avionics PLC systems, where bundles of cables are a common choice for wiring. We therefore consider our PLC channel to be a cylindrically bundled set of n phases plus a common return. Fig. 2 depicts the cross-section of such a wire with 3 phases.

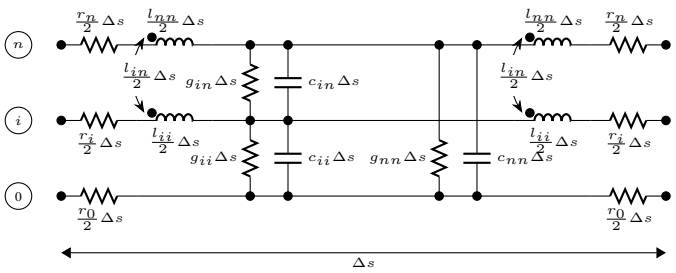

Fig. 3: T-model approximation of a transmission line segment of length Δs.

According to MTL literature [10], the mutual inductances (off-diagonal elements of $\boldsymbol{L}$) of such wire structures are given as

$$L_{ij} = \frac{\mu}{2\pi} \ln\left(\frac{d}{r_c}\right), \tag{15}$$

where μ denotes the magnetic permeability of the conductor material. The self-inductances (main-diagonal elements of $\boldsymbol{L}$) are given as $L_{ii} = \frac{L_{ij}}{2}$. The conductance and capacitance matrix $\boldsymbol{G}$ and $\boldsymbol{C}$ can be obtained from the relationships

$$\boldsymbol{G} = \mu\sigma\boldsymbol{L}^{-1} \tag{16a}$$

$$\boldsymbol{C} = \mu\varepsilon\boldsymbol{L}^{-1}, \tag{16b}$$

where σ and ε denote the conductivity and permittivity of the surrounding medium. The elements of the p.u.l. resistance matrix $\boldsymbol{R}$ are given as

$$R_{ii} = r_i + r_0 \tag{17a}$$

$$R_{ij} = r_0, \tag{17b}$$

where r_i denotes the resistance per conductor

$$r_i = \frac{\rho}{\pi(2r_c - \delta)\delta} \tag{18}$$

with the skin depth $\delta = \sqrt{\frac{2\rho}{\omega\mu}}$ (skin effect).

D. SPICE Model

For our SPICE simulations, we make use of lumped-element circuits, which are provided by MTL theory. For the lumped-circuit approximation to be applicable, the line segment has to be "electrically short", i.e., it has to be very short relative to the signal wavelength, usually $\mathscr{L} \ll \frac{\lambda}{20}$ [10]. Longer segments can be approximated by an N-fold concatenation of smaller segments that fulfill this criterion, i.e., $\mathscr{L} = N\Delta s, \Delta s \ll \frac{\lambda}{20}$. The reciprocal behavior of a transmission line can be achieved symmetrically arranging the lumped elements. We use a T-model in our implementation, as depicted in Fig. 3, where symmetry is achieved by arranging half of the longitudinal p.u.l. parameters (resistance, inductance) on each side of the transversal p.u.l. parameters (conductance, capacitance). The relationship between the p.u.l. matrices and the corresponding lumped-element parameters is well documented, e.g. by Paul [10].

TABLE I: Cable parameters of YSLY-JZ $4{\times}1.5\,\mathrm{mm}^2$ cable.

Conductor parameters			
r_c	t	ρ	μ
$0.69\,\mathrm{mm}$	$0.5\,\mathrm{mm}$	$1.995 \cdot 10^{-2}\,\Omega\,\mathrm{mm}^2/\mathrm{m}$	$\approx \mu_0$
Dielectric parameters		Experiment parameters	
ε	σ	$\mathscr{L}$	
$2.3 \cdot \varepsilon_0$	$1 \cdot 10^{-15}\,\mathrm{S\,cm/m}^2$	$1\,\mathrm{m}$	

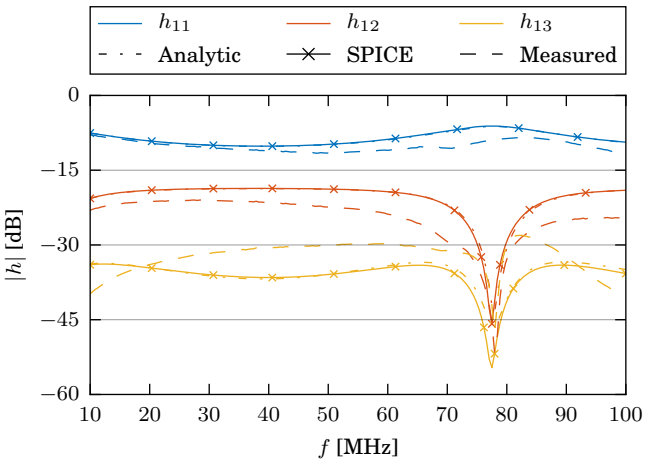

Fig. 4: Channel gains for a co-channel (h_{11}), cross-channel of adjacent phases (h_{12}) and of opposing phases (h_{13}) of a branchless connection with matched terminations ($100\,\Omega$).

E. Comparison of Analytical Results, SPICE Simulation and Measurements

Our measurements are performed on a YSLY-JZ $4{\times}1.5\,\mathrm{mm}^2$ cable with 3 phases and a neutral return conductor that serves as the reference conductor. Tab. I lists the parameters of this cable for our measurement setup.

Fig. 4 shows the comparison of the CTFs of our analytical results, SPICE simulations and measurements. The SPICE simulations have been carried out with perfect signal coupling. In order to obtain a cleaner plot we omit redundant CTFs by assuming channel reciprocity ($\Rightarrow h_{ij} = h_{ji}$), cable symmetry ($\Rightarrow h_{33} = h_{11}$, $h_{23} = h_{12}$), and small dimensions ($\Rightarrow h_{22} \approx h_{11}$).

We can make the following observations:

i) The analytical and SPICE-simulated results almost perfectly match, so the approximations made by the equivalent lumped-circuit have only little impact on the CTF.

ii) The measurements of the co-channels are fairly well aligned with our simulations, the cross-channels, however, show higher deviations, which are higher for the opposing channels h_{13} than for the adjacent channels h_{12}. We argue that the channel is generally susceptible to environmental influences, since the cable is not shielded, and especially the terminations and couplers are exposed to effects that we do not control. Also, we believe that highly attenuated channels are more susceptible to external conditions, which could explain the higher deviation for the opposing cross-channels, and more stable results for the co-channels.

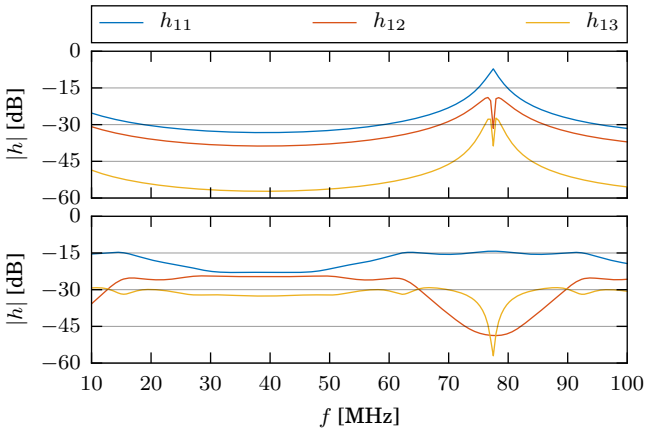

Fig. 5: SPICE-simulated CTF. Top: Branchless connection with low impedance ($1\,\Omega$) load. Bottom: Network with 3 branches and matched load.

Note that despite matched line terminations for all the phases, a deep fade is present at the cross-channels. Since we do not terminate the phases between each other, reflections occur at the cross-channels and generate the deep-fade through signal superposition.

F. Impact of Load Mismatch and Branches

In a realistic scenario, PLC systems will be exposed to varying loads; often a device suddenly draws high current, which can be modeled by a low impedance. Also, realistic PLC systems may operate on a network with several branches and nodes, rather than straight lines between only two nodes. Fig. 5 shows the impact of load mismatches (top), and of complex network topologies (bottom). Despite the overall higher attenuation, one important observation is that the relative "distance" between the co-channels and cross-channels decreases; this effect is stronger for the load mismatch than for the introduced branches.

This has two important implications to our safety-critical scenario: For optimal conditions, e.g., matched terminals (c.f. Fig. 4), the MIMO PLC channel approaches a scaled identity matrix, which is different from the wireless channel. Second, for non-optimal conditions, the amount of cross-talk increases. In the next section, we will investigate the impact of this change in cross-talk on the system performance in more detail.

III. Performance Evaluation of Different Multi-Conductor Systems

In order to evaluate the gains and limits of MIMO for safety-critical PLC applications, we evaluate and compare the system performance of three different systems that could potentially be deployed on top of a multi-conductor infrastructure: (1) a MIMO system, (2) n parallel SISO (nSISO) systems and (3) a

single SISO system. A key difference of the three considered systems is the role that cross-talk plays in each system: In a MIMO system, cross-talk provides the cross-channels and thus is utilized constructively. In nSISO systems, cross-talk creates interference between the parallel SISO systems and therefore has a negative impact. A single SISO system only operates on one phase and therefore no cross-talk is present. From an economical perspective, we consider the MIMO system to have the highest system complexity and thus the highest cost, while the SISO system has the least complexity and therefore the least cost. Unlike the wireless channel, PLC channels have much stronger co-channels, so we argue that nSISO systems are a cost-efficient alternative to a MIMO system. One can easily show that for perfectly isolated co-channels (no cross-talk), nSISO systems perform as well as a MIMO system, with the benefit of only n times deploying existing SISO systems and thus save costs.

A. Channel Capacity

Our performance evaluation is based on the channel capacity with the assumption of perfect channel knowledge at the receiver. We define the signal-to-noise ratio (SNR) $\rho = \frac{P_t}{P_n}$ to be the ratio of the total available transmit power P_t over the noise power P_n at the receiver[3]. We assume zero-mean Gaussian white noise at each receiver, and a multi-carrier system with subcarrier spacing B. The narrow-band MIMO channel capacity then amounts to [11]

$$C = B \sum_{i=1}^{R} \log_2 \left(1 + \frac{\rho}{N_t} \lambda_i^2\right), \tag{19}$$

where λ_i denotes the i-th singular value of the channel matrix and R its rank.

The SISO channel capacity is given by

$$C = \max_{i \in \{1,\dots,N_t\}} B \log_2 \left(1 + \rho |h_{ii}|^2\right), \tag{20}$$

where we chose the best channel among the n available channels.

For the nSISO mode, we have to account for the interference that is introduced by the cross-talk, which is contained in the off-diagonal channel gains $h_{ij}, i \neq j$. This yields a channel capacity of

$$C = B \sum_{i=1}^{N_r} \log_2 \left(1 + \frac{1}{\rho^{-1} N_t + \sum_{j=1, j\neq i}^{N_t} |h_{ij}|^2} |h_{ii}|^2\right). \tag{21}$$

Also note that for the MIMO and nSISO mode, the transmit power is equally distributed among the transmitters in order to have the same total transmit power for all systems and thus, maintain comparability. This is accounted for by the scaling factor $\frac{1}{N_t}$ in (19) and (21).

[3]Information theory introduces a normalization that allows a channel-independent interpretation of the SNR at the receiver. Since we are interested in comparing systems on the *same* PLC channel, we have to omit this normalization, as the scaling would be different for all three systems.

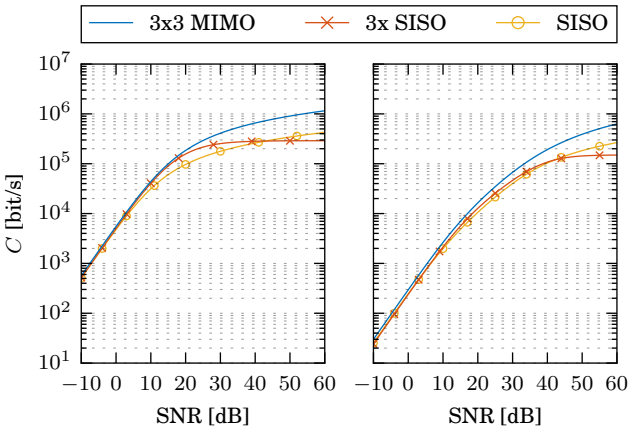

Fig. 6: Channel capacity for a direct connection beween two nodes with matched line terminations (left) and low impedance (1 Ω) terminations (right).

B. Impact of Load Mismatch and Branches

We consider a broad-band system, where we split the broad-band channel into multiple narrow-band subcarriers so we can make the flat-channel assumption for each subcarrier. The channel capacity presented in our results is the average channel capacity per subcarrier[4] with a bandwidth of $B = 25\,\text{kHz}$ each.

Fig. 6 shows the channel capacity of all three systems for a branchless connection with matched (left) and mismatched terminals (right). For the different SNR regions, we can make the following observations:

High SNR: The MIMO mode outperforms both the other systems for high SNR. With terminal mismatches the overall capacity decreases, but also, the MIMO gain decreases. The capacity of the nSISO system is limited as soon as the cross-talk dominates over the noise, and for increasing SNR the SISO system eventually outperforms the nSISO system.

Medium SNR: In case of matched terminals, there is a limited region in which the nSISO system performs better than the SISO system. As soon as the terminal is mismatched, this region vanishes and the performance of nSISO systems degrades below the SISO performance.

Low SNR: The SISO system is as performant as the nSISO systems. Since the capacity behaves linearly to the SNR ($\log(1 + x) \approx x$ for $x \ll 1$), it makes no difference whether the transmit power is distributed over many SISO channels or just one. The MIMO system has a little gain, but only in case of mismatched terminals. On the contrary, for matched terminals, we have reduced cross-talk (c.f. Sec. II-F) and thus almost no gain can be achieved with MIMO.

[4]Despite the context of worst-case considerations, taking the average over multiple subcarriers is a legitimate procedure since a realistic system would employ many subcarriers at the same time.

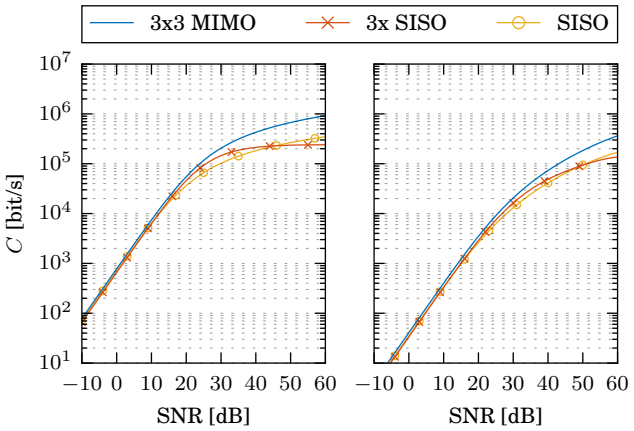

Fig. 7: Channel capacity for a connection with 3 branches and matched line terminations (left) and low impedance (1 Ω) terminations (right).

These observations confirm the findings from the Wireless and in-home PLC domain that MIMO provides gains over SISO. Even though there is little gain for low SNR, these gains vanish in worst-case; if a system is known to be operating under low SNR conditions, these little gains might not justify the higher costs of a MIMO system compared to a SISO system. The nSISO systems have only shown better performance than a SISO system, and in worst-case, there is no gain or even worse performance than the SISO system, which makes nSISO systems unsuitable for safety-critical applications. Nevertheless, PLC systems with non-safety-critical applications could exploit nSISO systems as a cost-efficient alternative to a MIMO system.

For increasing number of branches, the conclusions are similar to those with mismatches at the terminals. Fig. 7 shows the channel capacity for a network between two nodes with three equally spaced branches in between, again with matched (left) and mismatched terminals (right). In more complex network topologies, the cross-talk level rises (c.f. Fig. 4, 5), which has an impact on the channel capacity similar to mismatched line terminations. This underlines our findings that in realistic scenarios, nSISO systems do not provide significant gains over a single SISO systems.

IV. Conclusion and Outlook

In this paper, we evaluate the benefits and limits of MIMO technology for safety-critical PLC applications. Unlike other applications, safety-critical applications have to guarantee system performance for any operating conditions—including worst-case conditions. To do so, we present an extension to existing MTL-based channel models by incorporating terminal conditions, which in turn allows us to model performance degradation due to mismatches. We then use our channel model to compute the channel capacity and thereby evaluate the system performance. We can confirm the gains of MIMO technology over SISO technology, even for safety-critical PLC applications, however, we also show its limitations. Despite the gains for medium to high SNR, which are even achieved for bad matching conditions, these gains decrease for lower SNR and, in worst case, almost completely vanish. For low SNR, a SISO system provides a more cost-efficient alternative with only little performance loss compared to a MIMO system. We have also shown that although parallel SISO systems provide a cost-efficient alternative to MIMO systems, they perform worse than a single SISO system in worst case, which makes them unsuitable for safety-critical applications.

The comparison of our channel models to the measured channels have shown space for improving the accuracy. So far, we obtain the p.u.l. paramaters for our channel model from closed-form solutions, which are subject to simplifications, as already highlighted by Gruber and Lampe [9]. For more realistic configurations, finite-element methods could be employed to obtain the p.u.l. parameters. The SPICE-simulated channel models can be extended by more accurate circuit models for the signal couplers, which will further improve the accuracy of our channel model. Furthermore, a bigger measurement campaign would allow better verification of our channel models, and also provide a data basis for statistical channel analysis, which would increase the practical relevance.

References

[1] A. Schwager, D. Schneider, W. Baschlin, A. Dilly, and J. Speidel, "Mimo plc: Theory, measurements and system setup," in *IEEE International Symposium on Power Line Communications and Its Applications (ISPLC)*, 2011, pp. 48–53.

[2] D. Schneider, A. Schwager, W. Bäschlin, and P. Pagani, "European mimo plc field measurements: Channel analysis," in *IEEE International Symposium on Power Line Communications and Its Applications (ISPLC)*, 2012, pp. 304–309.

[3] L. T. Berger, A. Schwager, P. Pagani, and D. M. Schneider, Eds., *MIMO Power Line Communications: Narrow and Broadband Standards, EMC, and Advanced Processing*. CRC Press, 2014.

[4] S. Dominiak, L. Andersson, M. Maurer, A. Sendin, and I. Berganza, "Challenges of broadband plc for medium voltage smart grid applications," in *Workshop on Power Line Communications*, 2012.

[5] S. Dominiak, S. Serbu, S. Schneele, F. Nuscheler, and T. Mayer, "The application of commercial power line communications technology for avionics systems," in *IEEE/AIAA Digital Avionics Systems Conference (DASC)*, 2012, pp. 7E1–1–7E1–14.

[6] H. C. Ferreira, L. Lampe, J. Newbury, and T. G. Swart, *Power Line Communications—Theory and Applications for Narrowband and Broadband Communications over Power Lines*. John Wiley Sons, 2010.

[7] M. Zimmermann and K. Dostert, "A multipath model for the powerline channel," *IEEE Transactions on Communications*, vol. 50, no. 4, pp. 553–559, 2002.

[8] F. Versolatto and A. M. Tonello, "An MTL theory approach for the simulation of MIMO power-line communication channels," *IEEE Transactions on Power Delivery*, vol. 26, no. 3, pp. 1710–1717, 2011.

[9] F. Gruber and L. Lampe, "On plc channel emulation via transmission line theory," in *IEEE International Symposium on Power Line Communications and its Applications (ISPLC)*, 2015, pp. 178–183.

[10] C. R. Paul, *Analysis of Multiconductor Transmission Lines*, 2nd ed. Wiley-IEEE Press, 2007.

[11] J. R. Hampton, *Introduction to MIMO Communications*. Cambridge University Press, 2013.